



ORIGINAL ARTICLE

Chemical durability of lead crystal glass: Comparison of short-term aqueous and atmospheric alteration at 90°C

Marie Collin¹ | Babacar Diallo¹ | H el ene Lecoq¹ | Sandra Ory¹ |
Elodie Chauvet² | Nadia Pellerin¹ ¹CNRS, CEMHTI UPR3079, Univ. Orl ans, Orl ans, France²Tescan Analytics, Laboratory Analysis, Fuveau, France**Correspondence**Nadia Pellerin, CNRS, CEMHTI UPR3079, Univ. Orl ans, F-45071 Orl ans, France.
Email: nadia.pellerin@univ-orleans.fr**Funding information**

R egion Centre-Val de Loire, Grant/Award Number: VIVACE project

Abstract

Crystal glass alteration in an aqueous medium has been extensively studied following the implementation of strict regulations regarding lead leaching. However, despite the widespread use of lead glasses and crystal glass by artists and artisans ever since antiquity, few works focus on crystal glass corrosion in atmospheric conditions. In this preliminary study, the altered layers formed on crystal glass in aqueous and atmospheric conditions at 90°C are compared. On the timescale studied (20 days), ToF-SIMS profiles of both altered layers show water ingress. This hydration step is correlated with K leaching in aqueous media, and ²⁹Si and ²⁷Al NMR analysis of the altered structure highlights the formation of new *Q*⁴ and AlO₆ units. Low alkali leaching is observed in atmospheric conditions, but the altered glass structure is highly hydrolyzed, as attested by its high water and silanol content. As a result, the altered layer formed in aqueous conditions is more polymerized than the one formed in atmospheric conditions, and potentially more passivating through a mechanism involving water availability. On the bases of ²⁹Si/¹H and ²⁷Al/¹H CP-MAS NMR experiments, the oxygen repartition is described in the altered glasses, differentiating the oxygen atoms involved in structural NBO from that of hydroxyl groups.

1 | INTRODUCTION

Since its discovery during the 17th century, lead “crystal” glass has been used extensively. Its PbO content (24 wt% minimum¹) leads to a high refractive index. For this reason, crystal glass possesses a brilliance that is still valued nowadays for glass tableware. However, due to the hazardous nature of lead,² the use of crystal glass to produce containers for beverage consumption is currently the focus of scientific attention. New regulations such as Registration, Evaluation, Authorization, and Restriction of Chemicals (REACH) aim to lower the authorized limit of lead exposure.³ Standard experiments in acid conditions have thus been developed to assess lead leaching kinetics in solutions.^{4–10}

Literature on lead crystal glass alteration in aqueous and static conditions is scarce, and often limited to acidic conditions.^{5,6,10} The behavior of other types of silicate and borosilicate glass has been extensively studied in a variety of temperature and pH conditions.^{11–16} The general mechanisms of alteration in these types of glass are well established. The first step of hydration and ion interdiffusion^{17–19} is rapidly followed by the hydrolysis of the glass structure, that is, the so-called stage I of glass alteration when the glass is altered at its maximal rate *r*₀.^{11,14,19} The formation of altered layers (amorphous gel layer(s) and/or crystalline phases) at the surface of the glass due to solution saturation limits the glass alteration.^{20,21} Glass corrosion reaches stage II where alteration occurs at a residual rate much lower than *r*₀. During

this stage, the altered layer keeps on growing and evolving through mechanisms still debated (hydrolysis/condensation and/or dissolution precipitation),^{20–24} but its reorganization over time is assumed to limit water transport.²² Resumption of alteration due to secondary phase precipitation can sometimes be observed for specific glass composition at high pH. In the case of crystal glass, several studies performed in acetic acid solution have shown that the formation of the passivation layer is highly dependent on the S/V studied.⁵ The altered layer, when formed, is more polymerized than the pristine glass,^{5,25} and lead leaching was observed to be much less pronounced than alkali leaching.

Lead glasses with a large range of PbO concentrations have been widely used over time to produce objects and artworks currently kept in museums. Lead oxide significantly lowers glass transition and melting temperatures, and also reduces the expansion coefficient of the glass.²⁶ As a result, lead glazes have been used on ceramics since antiquity.²⁶ Many famous examples of ceramic artworks produced over time are covered by a lead glaze, such as Islamic enamel,²⁷ Bernard Palissy works,²⁸ or the “*Petit feu*” colors such as the one used at the French porcelain manufactory of *Sèvres*.²⁹ Moreover, some glass shaping techniques, such as lampwork, require the use of glass compositions with low transition and melting temperatures. Lampworked artworks, such as that known as *Verre de Nevers*, were therefore crafted using various types of lead glass.³⁰ Crystal glass itself has been used to produce artworks or decorative objects. Considering lead glass has a known tendency to be altered by aqueous water, one might wonder about its durability when in contact with water vapor.

Glass corrosion in atmospheric conditions is a topic of great interest to many communities. It has been extensively studied by the conservation community for various common glass compositions, such as soda lime or mixed-alkali silicate glasses.^{31–33} This type of corrosion has also been of interest to the nuclear glass community for several decades now in the context of nuclear waste immobilization in various borosilicate glass matrices.^{34–39} Due to unsaturated conditions, atmospheric glass alteration mostly leads to the formation of salt precipitates on top of a hydrated layer.³⁷ The hydrated layer thickness increases over time, and variation in relative humidity can affect the state of the glass surface.

The modification of the altered layer volume due to drying cycles can generate constraints leading to the formation of cracks.^{31,37} This can further enhance glass alteration: cracks are preferential pathways for water molecule diffusion.³² In spite of the conservation community interest for glass artwork durability, few studies actually focus on lead glass alteration in atmospheric conditions, that is the type of corrosion considered in a museum environment. Uncertainties thus remain regarding the durability of lead glass artworks in museums.

Comparing the altered layers formed in aqueous and atmospheric conditions can give access to new understanding of the alteration mechanisms. This methodology has been applied only for nuclear glasses to the best of our knowledge.^{34,40} The aim of this preliminary study is thus to present for the first time a comparison of the altered layers formed in atmospheric and aqueous conditions during crystal glass alteration. More specifically, a combination of complementary analysis techniques including ToF-SIMS profiling, TGA and NMR is applied to characterize the composition, hydration degree, and structure of each altered layer. The results give a new understanding of crystal glass behavior during alteration. The effect of various glass surface treatments on crystal glass behavior is also assessed and presented here.

2 | EXPERIMENTAL PROCEDURE

2.1 | The samples

All experiments were performed on a lead crystal glass with a PbO content of 30.2 wt% (Table 1).

Glass bubbles of ~100 g (Table S1) were prepared by a professional glassblower. The bubbles were blown from molten crystal glass (produced by Cristalica GmbH, Döbern, Germany), and annealed for 12 hours at 450°C. Several surface treatments, detailed in Table 2, were performed before or after annealing depending on the treatment considered.

The glass bubbles (~10 cm in diameter and 0.5 cm in thickness) were then cut to obtain monoliths. Glass homogeneity was verified using SEM-EDS imaging and analysis, and Raman spectroscopy mapping.

TABLE 1 Pristine crystal glass composition

	SiO ₂	Na ₂ O	Al ₂ O ₃	K ₂ O	Sb ₂ O ₃	PbO	
Wt%	53.2	4.0	0.5	11.4	0.7	30.2	
Mol%	73.0	5.3	0.4	10.0	0.2	11.1	
	Si	Na	Al	K	Sb	Pb	O
Wt%	24.9	2.9	0.3	9.5	0.6	28.0	33.8
At%	25.2	3.6	0.3	6.9	0.1	3.8	60.1

TABLE 2 Samples prepared for the experiments

No	Type of surface treatment	Type of sample
1	No surface treatment	For glass powder
2	No surface treatment	For monoliths
3	Sanding of the surface (After annealing)	For monoliths
4	Grinding of the surface (After annealing)	For monoliths
5	Silver foil deposited on the surface. (Before annealing)	For monoliths

A non-surface-treated crystal glass bubble was crushed into powder. The powder was prepared by sieving and decantation in acetone and ethanol to obtain a 2- to 4- μm -sized glass powder. SEM was performed on the powder to verify the size of the particles (Figure S1A).

2.2 | Alteration experiments in atmospheric conditions

Five hundred milligrams of 2- to 4- μm -sized glass powder, non-surface-treated monoliths, and surface-treated monoliths were placed in a climatic chamber at 90°C and 90% of relative humidity. The effect of light was not studied here, and the climatic chamber was left in complete darkness. A sample of each monolith was retrieved after 20 days. The glass powder was retrieved after reaching total alteration (~1 month). All samples were stored at room temperature and ambient relative humidity before characterization.

2.3 | Alteration experiments in aqueous conditions

All experiments were prepared in 500 mL perfluoroalkoxy reactors using deionized water (DIW) initially saturated with respect to SiO_2 (theoretical $C_0(\text{Si}) = 160 \text{ mg L}^{-1}$ at $\text{pH}_{90^\circ\text{C}} 7$). Crystalline SiO_2 was introduced under agitation at 90°C. The pH was raised to 10.5 using 300 μL of NaOH 32% until near-total dissolution occurred (experimental $C_0(\text{Si}) = 158 \text{ mg L}^{-1}$ after 21 days). The pH was then lowered back to 7 using 210 μL of HNO_3 65% and 150 μL of 0.5 N. Two hundred and fifty milligrams of the 2- to 4- μm -sized glass powder were then placed in the reactor ($S/V = 3.42 \text{ cm}^{-1}$ with $S_{\text{geo}} = 0.68 \text{ m}^2 \cdot \text{g}^{-1}$). The S/V usually controls the rate at which solution saturation is reached during stage I, but does not affect stage II alteration kinetics much. In silica-saturated conditions, glass alteration kinetics are thus supposed to be independent of the surface-area-to-solution-volume (S/V) and are time-dependent only. The experiment was replicated twice

and found to be reproducible (Figure S1B). A sample of each monolith (non-surface-treated and surface-treated, Table 2) was placed in third reactor within the same conditions. The morphology of the samples renders surface determination difficult due to their being cut from glass bubbles, but as noted above S/V has no impact on the experiment here. During the experiments, the pH was maintained around 7 (7.3 ± 0.6) by adding small quantities of a 0.5 N nitric acid solution.^{20,41} The solution was regularly sampled over time. The samples were filtered (0.45- μm cutoff). All elements were monitored over time by inductively coupled plasma atomic emission spectroscopy (ICP-AES; Thermo Scientific iCAP™ 6000 Series). The initial solution is Si saturated and contains a significant content of Na (~150 ppm). Pb and Al were undetected. Only K was thus accurately quantified.

The powder was retrieved after total alteration (a few days), dried for 2 hours at 90°C, then stored in ambient conditions. The monoliths were withdrawn after 20 days, quickly rinsed with DIW and blow dried.

2.4 | Solid analysis

Solid analyses were performed on monoliths, on the 2- to 4- μm -sized pristine glass powder, and on the 2- to 4- μm -sized glass powders altered in aqueous and in atmospheric conditions.

Due to the use of quartz instead of amorphous silica for Si saturation, a slight contamination of the glass powder altered in aqueous solution was observed (presence of undissolved quartz that represents ~3% of the total sample retrieved).

2.4.1 | Depth profiling analysis

ToF-SIMS analyses (IONTOF TOF 5) of the monolith sample were performed within a month of sampling. The curvature of the samples was low enough not to be an issue when placing the samples in the ToF-SIMS chamber. An O_2^+ ion beam was set at 2 keV and 690 nA and used for surface abrasion ($200 \times 200 \mu\text{m}^2$). The analysis was then provided by a Bi_1^{2+} ion sputtering beam (25 keV, ~1.7 pA, $50 \times 50 \mu\text{m}^2$) followed by ToF investigation of secondary ions extracted from the monoliths. The surface was neutralized during analysis by a low-energy electron flux (<20 eV). The depth of the final crater was measured using a 3D profilometer, allowing elemental profile depth calibration. The following profiles were selected for analysis: H^+ , SiOH^+ , Na_2^+ , $^{41}\text{K}^+$, Pb^+ , Sb^+ , Al^+ , and $^{29}\text{Si}^+$. Na^+ , K^+ , and $^{28}\text{Si}^+$ profiles were saturated, and thus not used.

H^+ , SiOH^+ , Na_2^+ , $^{41}\text{K}^+$, Pb^+ , Sb^+ , and Al^+ profiles were then normalized to that of $^{29}\text{Si}^+$ to avoid matrix effects.⁵ The

resulting data were normalized to the mean value calculated in pristine glass to extract semi-quantitative information. All of this was done using the following formula:

$$Jn_i^a = \frac{J_i^a / J_i^{Si^+}}{\frac{1}{n} \sum_p^n J_p^a / J_p^{Si^+}} \quad (1)$$

where Jn_i^a is the normalized intensity of an element a ($a = H^+$, $SiOH^+$, Na_2^+ , $^{41}K^+$, Pb^+ , Sb^+ , and Al^+), and J_i^a and J_p^a are the raw intensities measured at a point i of the profile and a point p of the pristine glass.

A method similar to the one proposed by Pons-Corbeau, Cazet⁴² for glow discharge mass spectrometry was recently found to be suitable for altered glass layer characterization using ToF-SIMS data.⁴³ This method usually requires the use of standards. Here, the underlying pristine glass is considered to be an internal standard. Briefly, the ToF-SIMS profiles obtained on the altered layer formed on a crystal glass sample, initially made of Si, Pb, K, Na, Al, and Sb, are considered. Provided that a sufficient number of data are gathered in the underlying pristine glass, it is possible to calculate the average intensity K^a measured for each element in the pristine glass:

$$K^a = \frac{1}{n} \sum_{p=1}^n J_p^a \quad (2)$$

where J_p^a is the raw intensity measured for the element a (as Pb^+ , $^{41}K^+$, Na_2^+ , Al^+ , Si^+ , and Sb^+) at a point p of the pristine glass.

The raw intensity J^a measured at any point of the profile is linked to the atomic concentration x^a of the element a . However, several unknown factors, such as emission yield for example, can have an impact on this intensity. Nevertheless, it is possible to eliminate those factors by using the following relation:

$$x_i^a = \frac{J_i^a \cdot [x_{PG}^a \cdot K^{Si} / x_{PG}^{Si} \cdot K^a]}{\sum J_i^a \cdot [x_{PG}^a \cdot K^{Si} / x_{PG}^{Si} \cdot K^a]} \quad (3)$$

where x_i^a is the atomic fraction of the element a (with $a = Pb, K, Na, Al, Si, \text{ or } Sb$) at a point i of the profile and x_{PG}^a is the theoretical atomic fraction of the element a in pristine glass, J_i^a is the raw intensity measured for the element a (as Pb^+ , $^{41}K^+$, Na_2^+ , Al^+ , Si^+ , and Sb^+) at this point i , and K^a is the average intensity in pristine glass calculated from equation (2) for each element a . The resulting profiles are fully quantitative, provided that no significant exogenous species were incorporated in the altered layer. Note that here, O was purposefully left out due to uncertainties regarding ToF-SIMS vacuum effect on aqueous species susceptible to evaporate. The O content from the structure was then calculated based on the other element content.

Both methods described above rely on the assumption that Si is the less mobile element in atmospheric and Si-saturated aqueous conditions, and can therefore be used to eliminate matrix effects.

2.4.2 | Thermogravimetric analysis

Thermogravimetric analysis (TGA) and Differential Thermal Analysis (DTA) analyses were performed on a SETARAM SETSYS Evolution 2400, under a flow of Ar in a platinum crucible. Two- to four-micrometer-sized pristine glass powder and glass powders altered in aqueous or atmospheric conditions were all analyzed (~50 mg each). A typical heating ramp of $10^\circ C \cdot min^{-1}$ was used between room temperature and $1200^\circ C$.

2.4.3 | X-ray diffraction

X-ray diffraction analysis was performed on the altered glass powders using a Philips X'pert Pro PANalytical instrument (Ni-filtered Cu $K\alpha$ source $\lambda = 1.5406 \text{ \AA}$) in a Bragg-Brentano geometry (from $2\theta = 20^\circ$ to $2\theta = 60^\circ$) to detect secondary phase formation.

2.4.4 | Raman spectroscopy

Raman spectroscopy was performed on the pristine and altered glass powders using a HORIBA Jobin Yvon T64000 that was equipped with a 514 nm excitation laser for a spectral acquisition between 400 and 1700 cm^{-1} to provide information regarding the pristine glass homogeneity, and to detect secondary phase formation after alteration.

2.4.5 | SEM analysis

Monolith samples were embedded in epoxy and polished with water using SiC sandpaper. SEM BSE imaging were performed on polished cross sections of monoliths altered 20 days in atmospheric or aqueous conditions using a Philips XL 40 ESEM microscope.

2.4.6 | NMR spectroscopy

NMR spectroscopy analyses were performed on the 2- to 4- μm -sized pristine glass powder and on the glass powders altered in aqueous or atmospheric conditions.

1H and ^{29}Si magic angle spinning (MAS) nuclear magnetic resonance (NMR) analyses were performed on a

Bruker Avance WB 400 MHz spectrometer (magnetic field 9.40 T). A Bruker 4-mm (external diameter of ZrO_2 rotor) cross-polarization magic angle spinning (CP-MAS) probe was used at a sample rotation frequency of 14 kHz. ^{29}Si NMR signal deconvolution was completed using the Dmfit program,⁴⁴ considering a Gaussian model line. The bridging and nonbridging oxygen numbers can be determined from the resulting Q^n repartition using the following equations⁴⁵:

$$\text{BO}(\%) = \frac{\%Q^4 \times 2.0 + \%Q^3 \times 1.5 + \%Q^2 \times 1.0 + \%Q^1 \times 0.5 + \%Q^0 \times 0.0}{\%Q^4 \times 2.0 + \%Q^3 \times 2.5 + \%Q^2 \times 3.0 + \%Q^1 \times 3.5 + \%Q^0 \times 4.0} \quad (4)$$

$$\text{NBO}(\%) = 100 - \text{BO} \quad (5)$$

$^{29}\text{Si}/^1\text{H}$ HETCOR 2D spectra were collected on the 2- to 4- μm -sized altered glass powders using contact times ranging from 0.75 ms to 14 ms

^1H MAS NMR signals were obtained from the altered crystal glasses by direct acquisition (DA) and using a Hahn echo (HE) pulse sequence with varying rotor-synchronized echo delays ranging from 71 to 17 857 μs . ^1H NMR signal deconvolution was completed using the Dmfit program,⁴⁴ considering a mixed Gaussian/Lorentzian model. Using the HE sequence data, the width and position of each contribution were fixed, and the amplitude was left free. Automatic optimization was run until reaching convergence. Note that the ^1H NMR spectra are often incompletely resolved due to the dipolar heteronuclear couplings and to the potentially strong intensity of the homonuclear dipolar couplings that can be induced by protons. The spinning rate can be insufficient to average these effects. As a result of this loss of resolution, the uncertainties associated with the fit are around ± 5 to 10% for the largest components.

^{27}Al MAS NMR spectra were collected on a Bruker Avance II 750WB spectrometer (magnetic field 17.62 T), using a Bruker 4-mm CP-MAS probe at a spinning frequency of 14 kHz. $^{27}\text{Al}/^1\text{H}$ CP-MAS NMR spectra were collected on the 2- to 4- μm -sized altered glass powders using contact times ranging from 0.75 ms to 3 ms. In total 40 000 scans were accumulated using a recycle time of 1s.

3 | RESULTS

In the following part, samples altered in aqueous conditions will be referred to as AQ samples. The ones altered in atmospheric conditions will be referred to as AT samples. ToF-SIMS profiling was performed to determine the chemical composition of the altered layer. Glass hydration was investigated by combining TGA and ^1H solid-state NMR. Both analyses are complementary: TGA provides quantitative

information on the overall quantity of the hydrated species present inside the sample regardless of their state (weakly or strongly bounded water molecule and hydroxyl groups), while NMR provides quantitative information regarding each individual species. Finally, the altered layer structure was compared to that of the pristine glass using ^{29}Si and ^{27}Al solid-state NMR.

3.1 | Solid analysis

3.1.1 | Chemical analysis

Chemical analysis of the altered layers formed in aqueous and atmospheric conditions were performed on 20-day-altered monolith samples using ToF-SIMS profiling. A comparison of the results highlights a difference in alteration behavior depending on the conditions after 20 days. The altered layer formed in aqueous solution is homogeneous in thickness, which is estimated to be between 5 μm (SEM observation, Figure S2A) and 6.8 μm (ToF-SIMS profiling, Figure 1A). In contrast, the altered layer formed in atmospheric conditions is only ~ 1.3 μm thick (ToF-SIMS profiling, Figure 1B). The interface between pristine and altered glass is particularly thin for the AQ sample and wide for the AT sample showing very different behavior.

The altered layer formed in aqueous conditions (90°C, pH_{90°C} 7, saturated with SiO_2) is homogeneous in composition, despite a gradient in K content ~ 0.25 to ~ 0.50 of K remaining). Surprisingly, Na appears to be unaffected. However, the initial solution contained ~ 40 ppm of Na (due to NaOH introduction for pH monitoring, see section 2.3 for more information), which might contribute to limiting Na leaching in solution as observed previously on borosilicate glass.⁴⁶ No significant Pb leaching is observed; Al and Sb are also unaffected. The altered layer is highly hydrated, as attested by the H^+ and SiOH^+ profiles (Figure 1C). The comparison of these profiles highlights the presence of both water molecules and silanol inside the altered layer: The H^+ profile average value is significantly higher than that of the SiOH^+ profile. No secondary phases are observed here on the extreme surface, an observation that is consistent with XRD analysis (Figure S3A,B).

The ToF-SIMS profiles obtained on the AT sample do not show drastic chemical changes (Figure 1B). K depletion ($\sim 40\%$) is observed. A Na enrichment at the surface, related to a low depletion in the altered layer suggests the precipitation of secondary phases. The altered layer studied here was not visible during SEM analysis on the cross section (SEM observation, Figure S2B) either due to the low chemical contrast between pristine and altered glass, or due to physical removal during water polishing. As a consequence, its homogeneity in thickness was not studied. No crystalline phases were detected when performing XRD and Raman analyses of

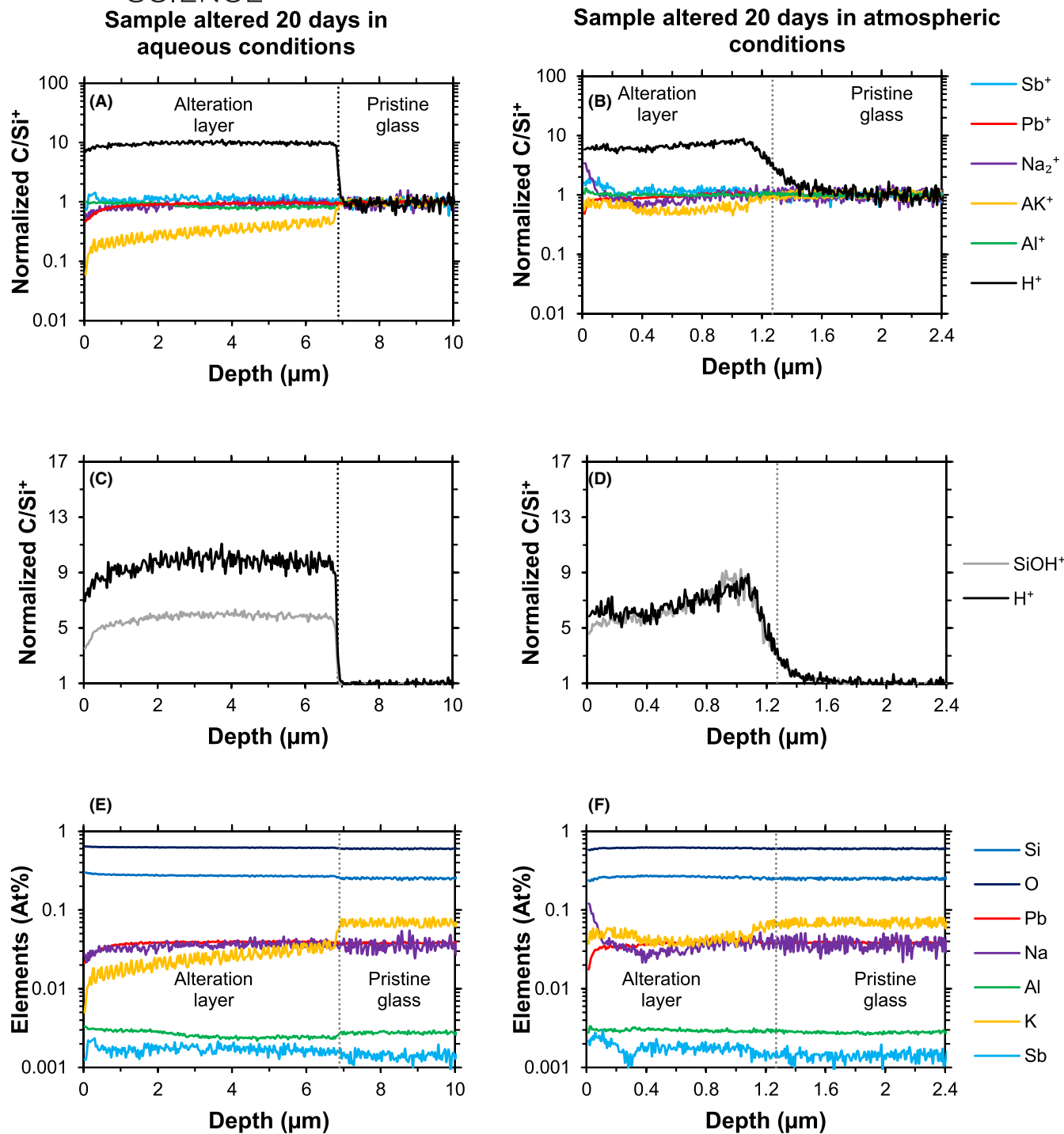


FIGURE 1 ToF-SIMS profiles obtained on samples altered 20 days in aqueous and atmospheric conditions (Color online). A and B, Comparison of each altered layer composition. Sb^+ , Pb^+ , Na_2^+ , $^{41}\text{K}^+$, Al^+ , and H^+ profiles are normalized to that of Si^+ (refer to Figure S4A,B for Si^+ raw profiles). C and D, Comparison of SiOH^+ and H^+ normalized profiles. E and F, Comparison of the ToF-SIMS profiles expressed in elemental concentration of the elements

the powder sample (Figure S3C,D), but the precipitation of amorphous secondary phases cannot be ruled out and has to be further investigated in future works. The perfect overlapping of the H^+ and SiOH^+ profiles (Figure 1D) suggests that most water molecules dissociate inside the glass structure to form silanol groups. The absence of water molecule signal

can also be imputed to the ToF-SIMS vacuum. It has been demonstrated that the vacuum has little effect on water molecule species in altered layers formed in aqueous conditions on borosilicate glass,⁴⁷ but it could affect differently lead glass samples altered in aqueous or atmospheric conditions. One way to avoid uncertainty in the future is to use cryogenic

preparation of the sample prior to SIMS analysis to avoid water evaporation.⁴⁷

Full quantitative profiles were calculated from the raw ToF-SIMS data using Equations (2) and (3). The profiles are relatively homogeneous in composition over the thickness of the layer (Figure 1E,F). The average composition of each altered layer can consequently be calculated (Table 3). Note that this composition does not consider exogenous species such as H.

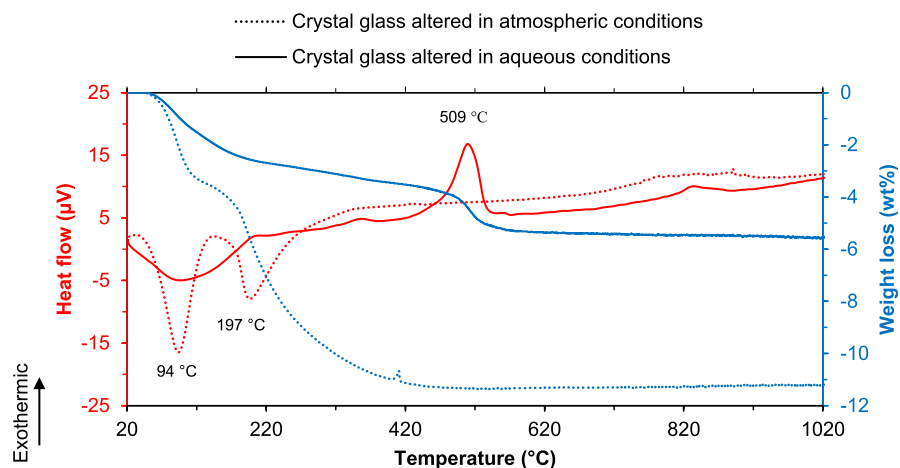
3.1.2 | Glass hydration analysis

The total water quantity inside the pristine and altered samples was determined using TGA. The amount of water found in pristine glass is below the quantification limit. AQ sample is hydrated up to 5.4 ± 0.1 wt%, and AT sample is hydrated up to 11.3 ± 0.1 wt%. The TGA curve comparison (Figure 2) shows that the AT sample contains more water molecules weakly interacting with the structure that easily evaporate around 90°C. This sample also contains more species that evaporate over 190°C (ie, mainly hydroxyls and potentially some water molecules strongly interacting with the porosity of the altered layer). The hydroxyl groups contained in the AQ are strongly bounded, and some need to reach a temperature of 508°C to totally condense and evaporate (Figure 2). This observation is consistent with a NMR study performed

TABLE 3 Pristine and altered crystal lead glass composition. Pristine glass composition was obtained using PIXE-PIGE analysis (error < 5%). The altered glass compositions were obtained from ToF-SIMS analysis (error < 15%)

Composition (at%)							
	Si	Pb	Na	Al	K	Sb	O
Pristine glass	25.2	3.8	3.6	0.3	6.9	0.1	60.1
AQ sample	27.6	3.7	3.5	0.3	2.3	0.2	62.5
AT sample	26.5	3.6	3.7	0.3	4.4	0.2	61.4

FIGURE 2 TGA and TDA data (Color online). The curves highlight the water evaporation process happening in both samples around 90°C. Silanol recondensation occurs mostly around 200°C for the AT sample, while the transition temperature of 509°C is required for the AQ sample, as attested by the exothermic peak in the TDA curve



on hydrated silica gel structure that shows the presence of isolated silanol groups at temperatures above 500°C.⁴⁸ However, a strong exothermic peak is correlated with the well-defined mass loss at 509°C. Dehydroxylation is usually associated with endothermic peak, as observed for phyllosilicates,⁴⁹ while exothermic peaks in amorphous material are generally associated with crystallization mechanisms.⁵⁰ No crystallization peak was observed for the pristine glass or the AT sample, and crystallization is not expected to happen in the AQ sample. Due to AQ low contamination in quartz (used for initial Si saturation of the solution), this peak could be related to the alpha to beta transition of the quartz structure. However, this transition is usually observed at 573°C, and while the N₂ atmosphere might reduce the temperature by up to 20°C, it would still happen at a higher temperature than that observed here. The phenomenon associated with this specific mass loss thus remains unclear.

Water speciation was further investigated using ¹H solid-state NMR spectroscopy. The main broad signal around 5 ppm in both samples is attributed to water molecules, as attested by the comparison of the spectra obtained without heat treatment and after a heat treatment of 12 hours at 90°C (Figure 3). The water signal decreases significantly after the drying procedure, especially for the AT sample. The quantities of desorbed water (~50% of both AT and AQ signals) are different to that observed during TGA analyses. However, TGA is performed under a flow of Ar that might favor water desorption prior to analysis. Moreover, a long drying procedure (12 hours at 90°C) favors the slower desorption kinetics of aqueous species that cannot be observed during TGA analysis due to the fast heating ramp (10°C·min⁻¹).

The presence of several hydroxyl groups can be noted in both samples. These hydroxyl groups (noted X-OH in Figure 3) are mostly silanol because of the low quantity of Al₂O₃ in the glass composition. Nearly all of those silanol units form hydrogen bonds (HB), as attested by their chemical shift above 5 ppm.²⁵ For the AQ sample, most of the silanol units' chemical shifts are comprised within a narrow

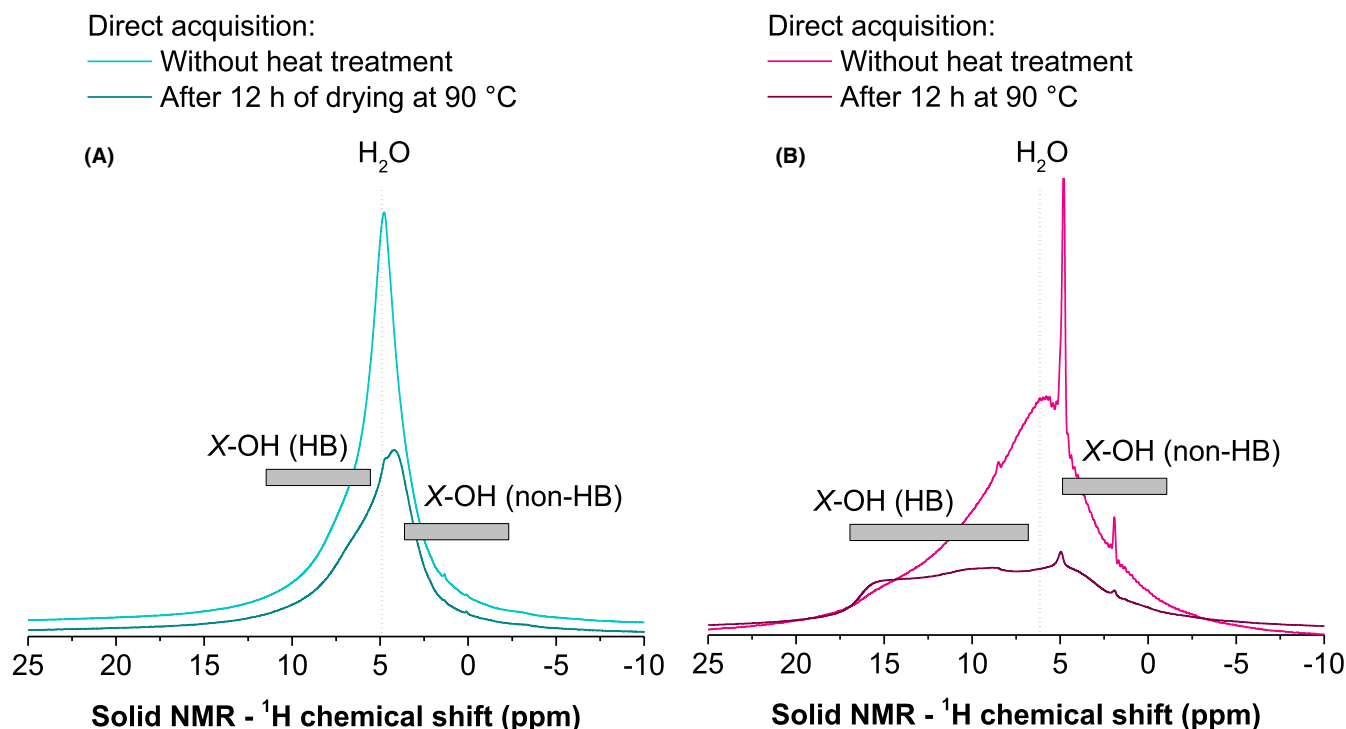
Sample altered 20 days in aqueous conditions**Sample altered 20 days in atmospheric conditions**

FIGURE 3 Solid ¹H MAS NMR signals obtained on altered samples at 750 MHz (Color online). A, Comparison between the signals obtained without heat treatment and after a heat treatment of 12 h at 90°C on the sample altered in aqueous conditions. B, Comparison between the signals obtained without heat treatment and after a heat treatment of 12 hours at 90°C on the sample altered in atmospheric conditions

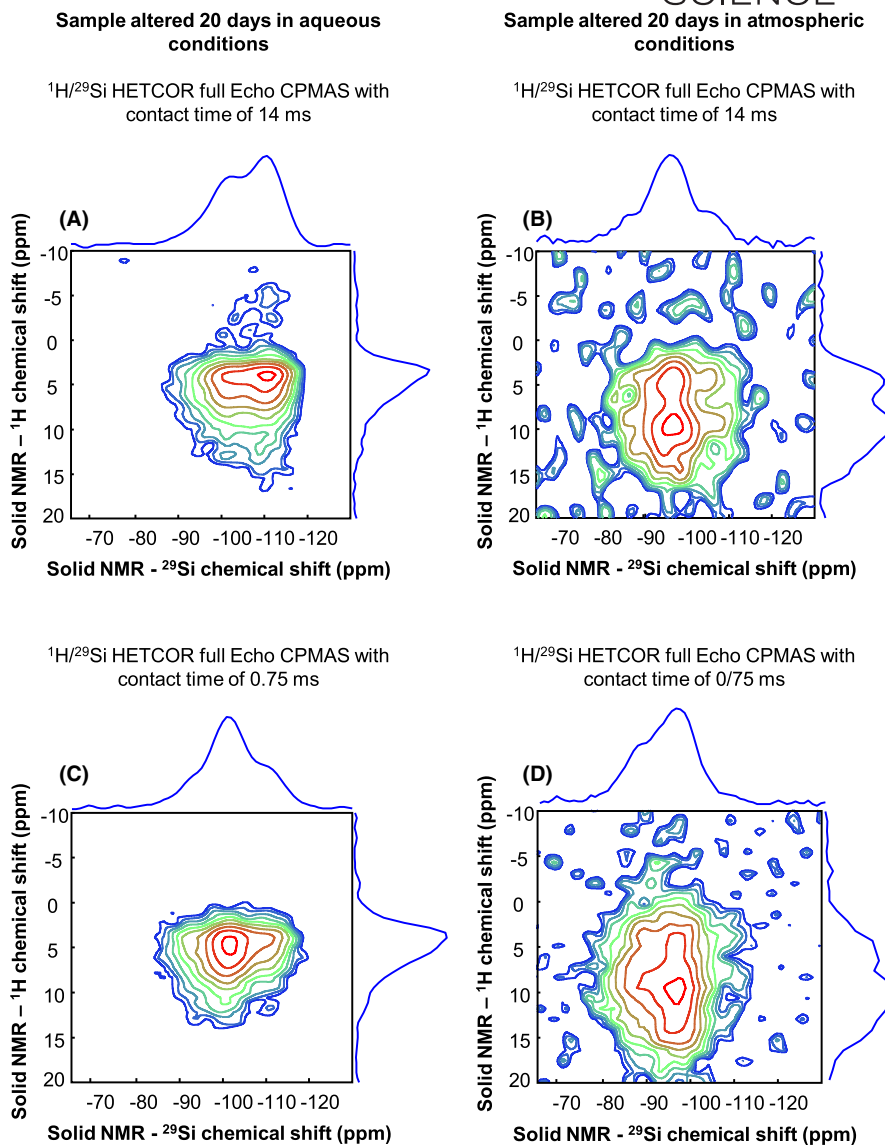
range, between ~5 and 10 ppm: most of the silanol groups inside the AQ sample have a similar environment. The ¹H/²⁹Si HETCOR experiments at two different contact times show a signal within the range -100, -110 ppm for silicon, depending on the contact time, and mainly correlated with Q⁴ species. They did not allow a further separation of any silanol groups such as Si(OH) or Si(OH)₂ (Figure 4A,C).

The silanol signal chemical shift range is broader for the AT sample (from ~6 to 18 ppm). This indicates the presence of several types of silanol groups with different environments. It is well-established that the chemical shift δ^H is strongly dependent on the H bonding strength of SiOH groups, which is directly correlated with the O-O distance.^{51,52} Here, a first strong signal is centered around 10 ppm, and a second signal is centered around 14 ppm. The ¹H/²⁹Si HETCOR experiments show a signal shifted toward the low fields compared to the AQ sample. This suggests a strong correlation between both of these Si-(OH) signals and all Qⁿ species (Q² and Q³, Figure 4C,D) and concerns mainly Q²-Q³ species at short contact angle. While similar signals have previously been observed in hydrated or altered glasses, their attribution is still debated.^{31,51,53} Alloteau, Lehuédé³¹ suggested that the signal near 10 ppm is that of silanol far from network modifiers

(ie, forming HB with bridging oxygen [BO] or oxygen from neighbor silanol groups), while the one at 14 ppm is that of silanol in close proximity of alkalis (ie, forming HB with non bridging oxygen [NBO]).^{31,53} In contrast, Le Losq, Cody⁵¹ suggested that the contribution near 10 ppm is that of silanol forming a hydrogen bond with NBO, while the signal above 15 ppm is attributed to SiOH forming intra-tetrahedral HB. While the exact attributions of the signals observed in our altered sample remain unclear, they indicate that the species observed here have different H bonding strength due to the altered layer composition. More specifically, the low alkali leaching compared to aqueous alteration results in a structure that is vastly different to that of AQ, which affects the bonding strength of the silanol groups due to modification of O-O proximity.

Some very sharp peaks can also be observed in each sample. Those signals are enhanced when using the HE sequences with long time delay (Figure S5A-C). The species considered here have long T2 relaxation time that indicates low H-H dipolar coupling. The shape of the spinning side bands also attests to the units assigned to these peaks' lower mobility (Figure S5D-G). The sharp signals around 1 ppm are usually attributed to minor isolated hydroxyl groups

FIGURE 4 $^1\text{H}/^{29}\text{Si}$ HETCOR full Echo CPMAS obtained on altered samples at 750 MHz. A and B, with contact time of 14 ms; favoring the signal of high Q^n species such as Q^4 . C and D, with contact time of 0.75 ms, favoring lower Q^n species such as Q^3 and Q^2 species



such as Si-(OH) or Al-(OH), that is, species that are non-H-bonded.^{25,52} This is consistent with the low H – H coupling observed here. The main signal centered around 4.8 ppm can either be attributed to surface hydroxyls,⁵⁴ to silanol bounded to water molecules in a very specific geometric environment,⁵⁵ or to water molecules strongly bounded to the silicate network.⁵⁵ The long relaxation time of this contribution, which suggests low H – H coupling, would tend to validate the first attribution. It is worth noting that this signal represents less than 3% of the total signal, and is thus a minor contribution.

The ^1H NMR signals of each altered sample were deconvoluted using a protocol described in supplementary material part 5. The HE sequence makes it possible to determine the number of contributions to consider, their width, and their position. The resulting proton repartitions are detailed in Table 4. The results obtained after drying the samples are consistent with TGA and ToF-SIMS analysis: the AT sample contains mostly silanol groups,

TABLE 4 Information extracted from NMR results. Proton repartition obtained from ^1H NMR spectra (error < 10%)

Proton repartition (% of H)			
	Thermal treatment	H from H_2O	H from X-OH
Pristine glass	None	—	—
Glass altered in aqueous conditions	None	89	11
	After 24 h at 90°C	72	28
Glass altered in atmospheric conditions	None	77	23
	After 24 h at 90°C	39	61

3.1.3 | Structural analysis of the pristine glass and the altered glasses

Structural analysis was performed on the 2- to 4- μm -sized powder of pristine and altered glasses using solid-state NMR spectroscopy (^{29}Si and ^{27}Al).

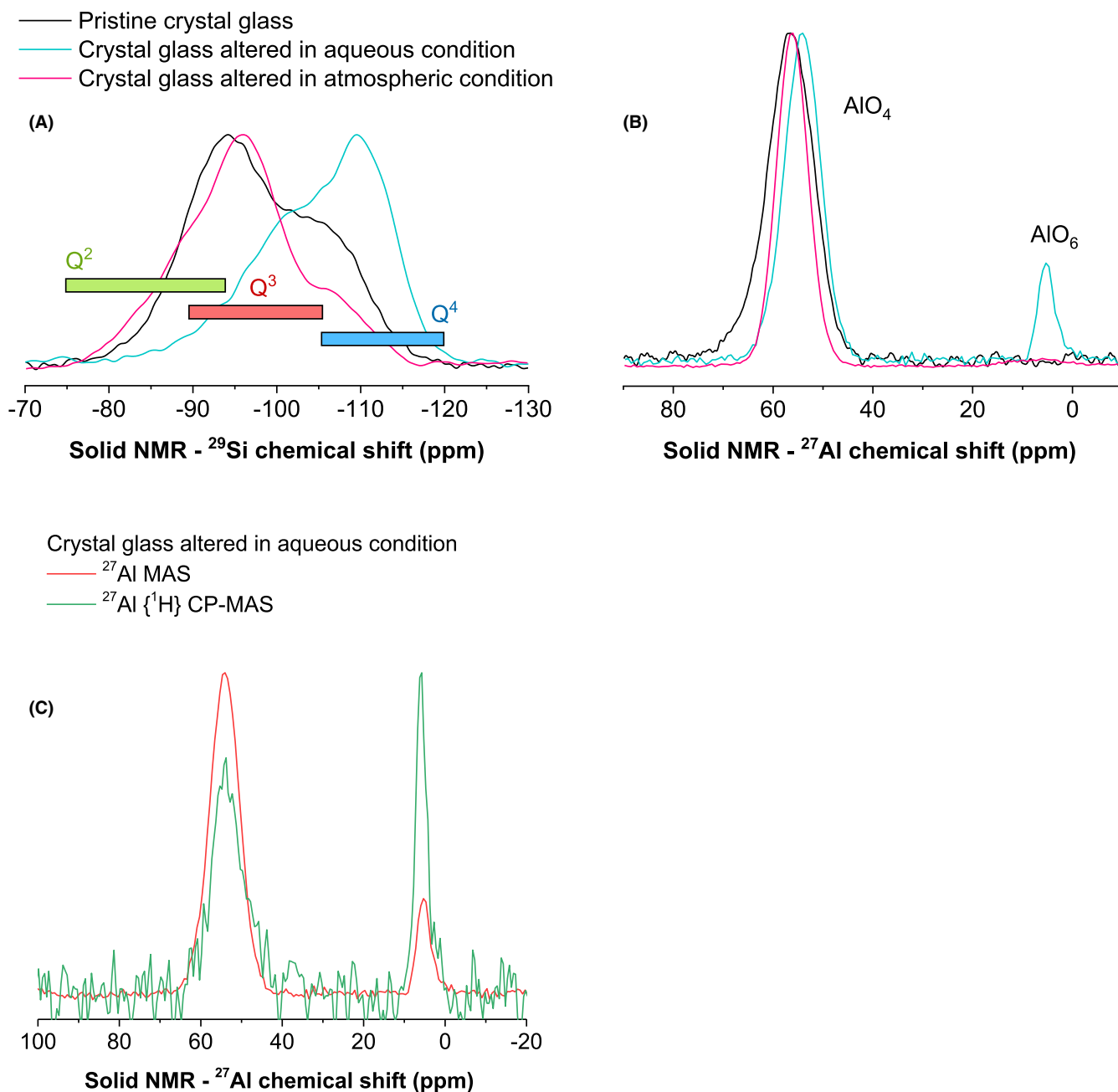


FIGURE 5 Structural comparison of pristine and altered glasses (Color online). All signals are normalized in intensity. A, ^{29}Si magic angle spinning (MAS) NMR signal of the 2-4 μm pristine and altered powders. Note that, for the AQ sample, a signal at -107 ppm, corresponding to a quartz contamination, was subtracted for better comprehension (Figure S7B). B, ^{27}Al magic angle spinning (MAS) NMR result. C, Comparison, for AQ sample, of ^{27}Al MAS and $^{27}\text{Al}\{^1\text{H}\}$ CP-MAS NMR spectra with a contact time of $0.75 \mu\text{s}$. No signal could be acquired for $^{27}\text{Al}\{^1\text{H}\}$ CP-MAS NMR with a contact time of $0.75 \mu\text{s}$ under reasonable acquisition time for AT sample

The ^{29}Si MAS spectra obtained for pristine and altered glasses show differences in the chemical shift δ^{Si} of the resonance (Figure 5A). This reveals differences in structure polymerization between pristine and altered glasses. Deconvolution of the pristine glass was performed assuming the presence of Q^3 and Q^4 species only (Figure S6A). Several $^{29}\text{Si}/^1\text{H}$ HETCOR analyses were performed on the altered samples to determine the number of contributions necessary

for signal deconvolution (Supplementary material part 7 and 8). The results highlight the presence of Q^2 , Q^3 , and Q^4 species in both AQ and AT samples (Figure 4). All the resulting Q^n repartitions are detailed in Table 5.

The AQ sample contains more Q^4 species than the pristine glass. However, it also contains Q^2 species that were not present in the pristine sample. A shift of δ^{Si} is observed for the Q^4 species between pristine and altered sample (Figure 5A). This

TABLE 5 Q^n and oxygen repartition inside the pristine glass and inside the altered layer formed in aqueous conditions and in atmospheric conditions (from data obtained without heat treatment). O_{NBO} refers here to the NBO chemically bound to network modifiers

Q^n repartition (%)						
	Q^2		Q^3		Q^4	
	δ^{Si} (ppm)	(%)	δ^{Si} (ppm)	(%)	δ^{Si} (ppm)	(%)
Pristine glass	—	0	-96 ± 1	68	-107 ± 1	32
Altered glass in aqueous conditions	-92 ± 1	13	-101 ± 1	29	-110 ± 1	58
Altered glass in atmospheric conditions	-87 ± 1	26	-96 ± 1	59	-107 ± 1	15

Total oxygen repartition (% of O) without heat treatment				
	O_{BO}	O_{NBO}	O_{OH}	$O_{\text{H}_2\text{O}}$
Pristine glass	70	30	—	-
Altered glass in aqueous conditions	71	16	3	10
Altered glass in atmospheric conditions	49	20	12	19

Structural oxygen repartition (% of O) without heat treatment			
	O_{BO}	O_{NBO}	O_{OH}
Pristine glass	70	30	0
Altered glass in aqueous conditions	80	17	3
Altered glass in atmospheric conditions	61	25	14

is attributed to the changes in composition, more specifically the leaching of K,⁵ to the reorganization of the network to a higher degree of polymerization in general, and to the change of Al-O-Si connectivity to a lesser extent. The replacement of AlO_4 by SiO_4 in $Q^n(\text{mAl})(\text{n-mSiO}_2)$ units is responsible for a well-known shift toward lower δ^{Si} ,⁵⁶ while chemical modification and repolymerization of the network have also been shown to induce a similar shift toward lower δ^{Si} .^{5,20,41}

No significant shift of δ^{Si} is observed in the AT sample (Figure 5A). This is consistent with the fact that its composition remains closer to that of the pristine glass compared to the AQ sample, hydration notwithstanding. However, the AT sample is more depolymerized than its pristine counterpart, as attested by the decrease in Q^4 species quantity and the increase in Q^3 and Q^2 species quantities (Table 5).

The ^{27}Al MAS spectra obtained for pristine glasses reveal that only AlO_4 units are present in the pristine structure (Figure 5B, Figure S6B and Table S6). In contrast, both AlO_4 and AlO_6 units are present in the altered samples. However, the AlO_6 units are much more prominent in the AQ sample (13.5%, Figure 5B and Figure S7C) than in the AT sample (4%, Figure 5B and Figure S8C). The δ^{Si} , the chemical shift distribution (Δcs), and the quadrupolar coupling constant (CQ) found for the AlO_6 units formed in AQ sample are lower than that found in the AT sample (Table S7 and Table S8). This tends to indicate

that the AQ AlO_6 units are much more homogeneous in geometry and chemistry. The AQ AlO_6 units also are favored during $^{27}\text{Al}/^1\text{H}$ CP-MAS NMR experiments compared to their AlO_4 counterparts (Figure 5C). This suggests that the octahedral units hold more hydroxyl groups than the tetrahedral ones.

Moreover, the AlO_4 unit signal obtained for the AQ sample is slightly shifted and sharper in the altered sample compared to that of the pristine one, although its symmetry does not change much. This is confirmed by its δiso , Δcs , and CQ obtained by fitting the spectra (Table S7). Similarly, the signal obtained for the AT sample is sharper due to the lower chemical shift distribution (Δcs). However, it is not shifted, and its symmetry is unchanged, as confirmed by its δiso and CQ (Table S8). The sharpening of the AlO_4 signal in an altered glass sample is usually attributed to the hydrated environment surrounding the units, that is exacerbated here for the AT sample. However, a modification of the chemical shift tends to indicate a change in the cation nature of the charge compensation. This is consistent with the leaching of alkali observed in the AQ sample.

Knowing the samples' composition, hydration degree, and water speciation, it is possible to calculate the oxygen repartition inside the samples (refer to Supplementary materials part 9 for more information on the calculation).⁴¹ The results for samples without thermal treatment are displayed in

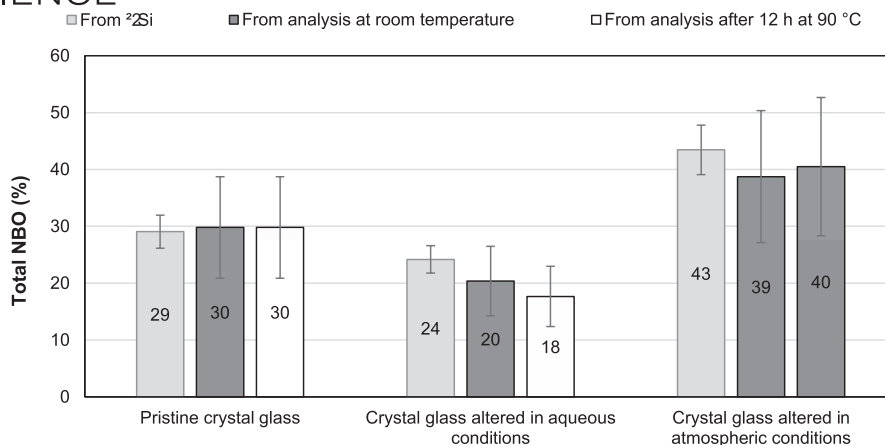


FIGURE 6 Total NBO quantity in pristine and altered glasses obtained without heat treatment and after 12 h at 90°C. No silanol condensation is usually observed at such a low temperature, the NMR Q^n repartition is thus expected to remain similar.⁴¹ The NBO quantities are expressed in percentage of oxygen in the structure. In all cases, NBO contents were calculated from both ²⁹Si NMR spectra and from sample analyses by ¹H NMR (NBO from hydroxyl –OH) and ToF-SIMS profiling (NBO chemically bound to network modifiers)

FIGURE 7 SEM images obtained on (A) a non-surface-treated sample, (B) a sanded sample, (C) a ground sample, and (D) a sample with silver foil on its surface, all altered 20 days in aqueous solution. The resin is in black, the altered layer appears in dark gray and the pristine glass in light gray

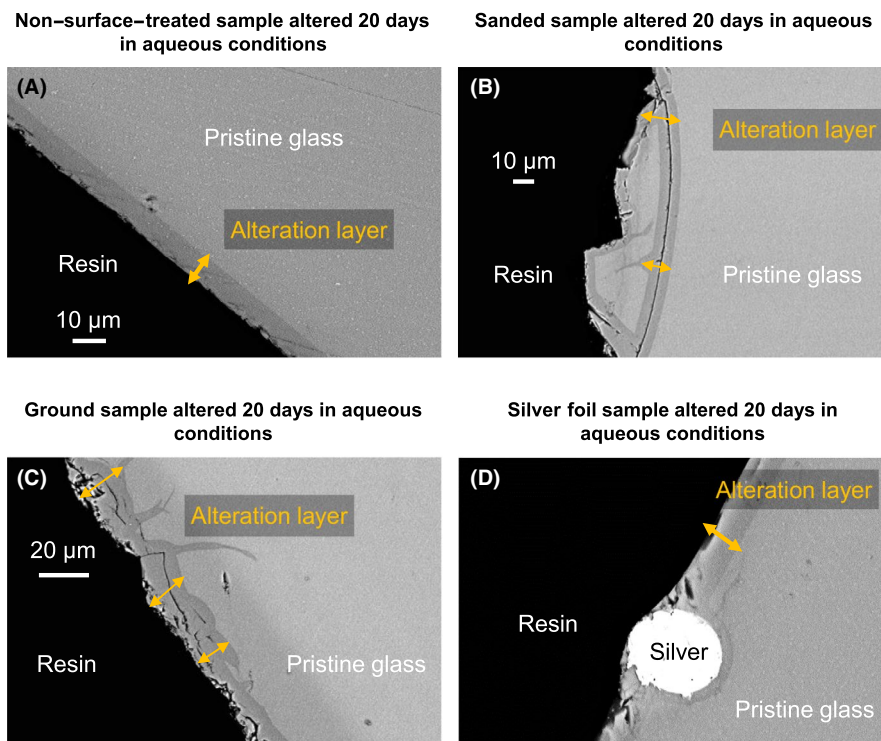


Table 5 (refer to Table S9 for results obtained on the samples heated for 12 hours at 90°C). The total NBO quantity calculated (comprising both NBO formed by network modifiers and silanol groups, and neglecting the Al-OH formed due to the low Al content of the glass) is compared to that obtained from ²⁹Si NMR analysis (Figure 6). The NBO quantifications are consistent for all samples within uncertainty, which validates the method and the various ¹H and ²⁹Si deconvolutions presented here. The slight NBO underestimation from analysis can be related to the difficulty to accurately subtract hydroxyl signals from that of water in the ¹H NMR signal obtained, especially in the AQ sample.

3.2 | State of the glass surface effect on glass alteration

Several physical surface treatments (sanding, grinding, and silver foil) were tested to assess their impact on the crystal glass durability. The treated samples were altered 20 days either in aqueous or in atmospheric conditions. The AQ samples were characterized using SEM imaging. Some images are presented in the paper, more are available in Supplementary materials part 10. The AT samples could not be characterized using SEM: either the absence of chemical contrast between the altered layers and the pristine glass is limiting the imaging,

TABLE 6 Thickness of the altered layer formed on non-surface-treated and surface-treated samples

	Aqueous conditions	Atmospheric conditions
No surface treatment	$5.0 \pm 0.3 \mu\text{m}$ of alteration ^a	$\sim 1.3 \mu\text{m}$ of alteration ^b
Sanding	$7.0 \pm 3.3 \mu\text{m}$ of alteration ^a	Nonvisible in SEM
Grinding	$9.4 \pm 3.6 \mu\text{m}$ of alteration ^a	Nonvisible in SEM
Silver foil	No silver: $6.0 \pm 0.3 \mu\text{m}$ of alteration ^a With silver: $2.2 \pm 0.4 \mu\text{m}$ of alteration ^a	Nonvisible in SEM

The thicknesses were determined either from ^a SEM analysis or ^b ToF-SIMS profiling.

or the layer was removed during sample preparation (water polishing).

Two treatments, sanding and grinding, result in the formation of microcracks that enable water diffusion deeper in the glass structure. As a result, their altered layer's morphology is very heterogeneous compared to that of non-surface-treated samples (Figure 7A-C). The alteration depth can reach up to 12 μm in aqueous solution (Table 6). In some zones, residual pristine glass islets are visible between altered regions (Figure 7).

Finally, the sample covered with silver foil presents interesting singularity. The silver tends to concentrate on the glass surface as microparticles that limit water diffusion (Figure 7E). As a result, the zones covered with silver particles are less altered in aqueous conditions than the noncovered one (Table 6).

4 | DISCUSSION

4.1 | Effect of the alteration conditions on the altered glass formation

The chemical and structural characterization of the altered layers formed in aqueous or atmospheric conditions at 90°C shows that the alteration conditions have a significant effect on the altered layer composition, hydration degree, and structure.

No crystalline secondary phases were detected by XRD or Raman spectroscopy on the aqueous or atmospheric treated samples, despite some Na enrichment being observed at the surface of the AT sample. The composition of the pristine glass (no Ca, Zn, Fe, and Ni, low Al content) and the conditions studied (near-neutral pH) do not favor the formation of secondary phases in aqueous conditions. No CSH, phyllosilicate or zeolite formation can be expected, contrary to what

is sometimes observed on nuclear glasses.^{57–59} In contrast, salts such as sodium or potassium carbonates, nitrates, sulfates, etc, are frequently observed on a glass surface during atmospheric corrosion.^{31,53,60–62} The first hypothesis to explain why no such phases are observed here is that the low Na₂O content in the glass studied (4 wt%) results in sparse secondary phase formation compared to other experiments performed on glass with higher Na₂O content. This would result in difficulty to obtain a diffraction pattern or a Raman signal for reasons of sensitivity. The second hypothesis is that the secondary phases forming are amorphous. Such phases cannot be detected by XRD analysis, but might be detected using Raman spectroscopy, provided that their signal can be separated from that of the altered structure. This needs to be further investigated, as no phases, amorphous or crystalline, were observed by SEM. It has to be noted that secondary phase precipitation is strongly dependent on temperature and time.⁵³ While no crystalline phases were detected here, secondary phase precipitation might be observed over a longer time scale, and/or at different temperatures.

No Pb, Si, Al, or Sb release is observed in aqueous or in atmospheric conditions (Figure 1). The altered layer formed in aqueous conditions is more depleted in K than the layer formed in atmospheric conditions. It is also much less hydrated (5.4 wt% compared to 11.3 wt%), which might appear counterintuitive at first: alkali leaching is usually expected to be linked to an interdiffusion phenomenon where alkali ions are exchanged with protonated aqueous species.^{11,20,41} However, the hydrated layer of the AQ sample structure also shows significant evidence of a reorganization phenomenon not observed in atmospheric conditions. This explains why this sample is less hydrated, as will be explained below.

AQ sample ²⁹Si NMR signal points out the presence of new Q^2 species that were not present in the pristine glass. This highlights the breakage of Si-O-Si bonds to form silanol groups, either by complete dissolution or by hydrolysis of SiO₄ units.^{21,23,24} The formation of AlO₆ units is also observed in the AQ sample. AlO₆ was not observed on aluminoborosilicate glasses altered in similar aqueous conditions,^{41,46} but was observed on the surface of aluminosilicate glasses and minerals altered in acid aqueous conditions.⁶³ This change of coordination from AlO₄ to AlO₆ is usually considered to be a first step in the dissolution of Al species.⁶⁴ Alkali leaching also affects the remaining AlO₄ units: The AQ signal is slightly shifted compared to that of the pristine sample, suggesting a change of the main charge compensator. Na is more retained in the AQ altered layer than K, and larger alkalis are known to affect the chemical shift and the quadrupolar coupling of the ²⁷Al signal of aluminosilicate glasses.^{47,65} Both ²⁹Si and ²⁷Al NMR results point out that the network has been significantly hydrolyzed and/or dissolved. Yet, the formation of new Q^4 units from lower Q^n species by re-condensation or by precipitation, and the overall

higher degree of polymerization of the network compared to the pristine glass indicate that the structure has been significantly reorganized following hydrolysis. Due to the chemical and structural modifications observed in aqueous conditions, the remaining Si-OH signal observed in NMR is very narrow (Figure 3). While several X-OH contributions are undoubtedly present in the ^1H NMR AQ signal, their chemical shifts are close: most silanol groups that formed have condensed, as explained above, and the remaining silanol groups have a very similar environment. The end results of aqueous alteration is thus a polymerized structure with a low silanol content, that still contains some water molecules, although their mobility might be hindered by the network reorganization, as observed in other studies.^{22,66}

In contrast, the AT does not show much evidence of network reorganization. The sample ^{29}Si NMR signal points out a strong hydrolysis/dissolution of the network. A significant decrease of Q^4 and Q^3 species proportion is observed, while new Q^2 species are formed. A low quantity of AlO_6 units is also detected, as observed previously on various aluminosilicate glasses altered in atmospheric conditions.⁶⁷ The AlO_4 units show little modified, in accordance with the low degree of alkali leaching observed. The resulting altered structure still retains 82% of its original NBOs (note that the AQ sample only retains 59% of it), and a significant fraction of new NBOs/silanol groups are formed by the hydrolysis of the network (Table 5). Due to the lower alkali leaching and the absence of repolymerization, the Si-OH signal observed in the AT sample is broad. Many silanol groups are present (Table 5) and their environment diversity (presence of BO, NBO from alkali, X-OH, etc) affects their H bonding strength and their chemical shift. This hydrated, nonpolymerized, structure might not be as passivating as that formed in aqueous conditions. Further studies could be carried out to explore the secondary phase formation and the passivating properties on longer durations.

The results obtained here in aqueous and atmospheric conditions suggest that the repolymerization mechanism and K leaching mechanism are correlated. A crystal glass of close composition, altered in acidic conditions, showed even higher network modifier leaching (K, Na, and Pb) and a higher degree of repolymerization than that observed in our study.⁵ In contrast, low alkali depletion and high network depolymerization have been observed on alkali-lime silicate glass altered in atmospheric conditions (80°C and 85% of relative humidity).^{31,53,67} Both mechanisms thus appear to be affected by water molecule propensity to dissociate to form protonated species, a phenomenon enhanced by 1) the pH of the solution, as observed by Angeli, Jollivet,⁵ and 2) the number of water molecule available, that is the saturation degree in atmospheric conditions. It thus seems that the initial water availability strongly affects the alteration mechanism: high water availability (ie, saturated condition) favors both

structure hydrolysis and ion exchange mechanisms, both of which are followed by structural reorganization. In contrast, lower water availability (ie, atmospheric conditions with $\text{RH} < 100\%$) promotes hydrolysis mechanism over ion exchange mechanism, which results in low to no reorganization of the structure. Network reorganization might happen, but would require higher water content. This might be observed at longer timescale when more water molecules have been able to enter and react with the structure, or at higher RH when more water molecules can condense at the glass surface. Further analyses at different RH using isotopes such as ^{18}O or ^{17}O are required to verify this hypothesis.^{22,23} Moreover, different glass compositions might also react differently: the structure of the glass itself might limit more or less water ingress and mobile species movement depending on its polymerization degree.^{66,68}

4.2 | Surface treatment effect on glass alteration

Three surface treatments were studied. One of them (the silver foil) appears to slightly reduce glass corrosion, but only on limited zones where silver microparticles form on the glass surface. This effect must be further studied, as no result could be acquired in atmospheric conditions. In the case of strong glass hydration followed by cracking and flaking of the surface, this beneficial effect might be quickly canceled, and could result in the loosening of the silver particle. This could significantly modify the physical appearance of the silver-coated glass surface.

The sanding and the grinding of the surface had the most impact on glass durability. Both treatments result in the formation of microcracks on the surface observed before the alteration treatment. Those cracks allow for a deeper water penetration inside the pristine glass,⁶⁹ resulting in the formation of an altered layer highly heterogeneous in thickness, with pristine islands in between altered layers sometimes observed. These observations are consistent with other studies on glass surface preparation and glass alteration.^{70,71} However, those studies also pointed out that, in aqueous conditions, the glass alteration enhancement effect tends to decrease over time.^{69,70} Moreover, in atmospheric conditions, the further cracking and flaking of the altered surface might surpass the effect of the microcracks formed prior to the alteration on glass durability over time.

In conclusion, the various surface treatments studied here might present some effects on glass durability, although more sensitive in the short term. It is probable that, in the long term, these effects will be in competition with other phenomena, resulting in a glass durability that could eventually be like that of a non-surface-treated glass.

5 | CONCLUSION

This study provides the first comparison of the alteration layers formed in atmospheric and aqueous conditions for a lead crystal glass. Overall, it is shown that “saturated” conditions (ie, aqueous conditions compared to atmospheric conditions below 100% RH) promote the leaching of alkali and a network reorganization following the hydration of the structure. In contrast, in the atmospheric conditions studied here (90% RH and 90°C), lower alkali leaching is observed and the network is highly hydrolyzed with little to no sign of repolymerization. This suggests that water availability in the glass structure is fundamental for the repolymerization mechanisms to be observed during glass alteration.

The current results were acquired at 90°C, and cannot be directly transposed to room temperature. Further studies are thus needed to deepen the understanding of crystal artwork durability in a museal environment, taking into account more variables than that studied here, such as temperature, humidity, light, or pollutants that can all significantly affect glass durability. The altered layer formation mechanisms in aqueous and atmospheric conditions could be further investigated in the future using ¹D and ¹⁸O or ¹⁷O isotopes.

ACKNOWLEDGMENTS

This work was supported by the Région Centre-Val de Loire within the framework of the VIVACE project. The authors are grateful to Pierre Gallou and Annie Duval (Verrerie d'Art d'Amboise Chargé) for the lead crystal glass samples preparation, and to PrimeVerre, Pierre Florian (CNRS), Vincent Sarou-Kanian (CNRS), Marianna Porcino (CNRS), César Leroy (CNRS), and Loïc Marchetti (CEA) for technical support and scientific input. The authors also thank the anonymous reviewers who greatly helped to improve the quality of the present manuscript, and Jane Raymond who proofread the final version of the manuscript.

AUTHOR CONTRIBUTIONS

NP supervised the study. MC was responsible for designing the study, experimental analysis and data interpretation, and writing the paper. BD designed and performed NMR experiments. HL performed SEM analysis. SO performed TGA and DTA analysis. EC performed ToF-SIMS analysis. All the authors helped on paper editing.

DATA AVAILABILITY STATEMENT

The data that support the findings of this study are available from the corresponding author upon reasonable request.

ORCID

Marie Collin  <https://orcid.org/0000-0002-0571-5019>

Babacar Diallo  <https://orcid.org/0000-0003-1400-9463>

Nadia Pellerin  <https://orcid.org/0000-0002-9436-3480>

REFERENCES

1. Council Directive 69/493/EEC of 15 December 1969 on the approximation of the laws of the Member States relating to crystal glass, 69/493/EEC (15 december 1969).
2. Needleman HL, Bellinger DC. Lead Hazards and Poisoning. 2017;377–83.
3. Registration, Evaluation, Authorization and restriction of CHemicals (REACH), 2006.
4. ASTM International. Standard Test Method for Lead and Cadmium Extracted from the Lip and Rim Area of Glass Tumblers Externally Decorated with Ceramic Glass Enamels. West Conshohocken, PA2014.
5. Angeli F, Jollivet P, Charpentier T, Fournier M, Gin S. Structure and chemical durability of lead crystal glass. *Environ Sci Technol.* 2016;50(21):11549–58.
6. Guadagnino E, Gambaro M, Gramiccioni L, Denaro M, Feliciani R, Baldini M, et al. Estimation of lead intake from crystalware under conditions of consumer use. *Food Addit Contam.* 2000;17(3):205–18.
7. Bertoncetto R, Milanese L, Bouquillon A, Dran JC, Mille B, Salomon J. Leaching of lead silicate glasses in acid environment: compositional and structural changes. *Appl Phys A.* 2004;79(2):193–8.
8. Rahimi RA, Sadrnezhaad SK. Effects of Ion-exchange and hydrolysis mechanisms on lead silicate glass corrosion. *Corrosion.* 2012;68(9):793–800.
9. Rahimi RA, Sadrnezhaad SK, Raisali G, Hamidi A. Hydrolysis kinetics of lead silicate glass in acid solution. *J Nucl Mater.* 2009;389(3):427–31.
10. Bonnet C, Bouquillon A, Turrell S, Deram V, Mille B, Salomon J, et al. Alteration of lead silicate glasses due to leaching in heated acid solutions. *J Non Cryst Solids.* 2003;2003(323):214–20.
11. Bunker BC. Molecular mechanisms for corrosion of silica and silicate glasses. *J Non Cryst Solids.* 1994;1994(179):300–8.
12. Bunker BC. Waste glass leaching: chemistry and kinetics. In: Bates JK, Seefeldt WB, editors. *Scientific Basis for Nuclear Waste Management X.* Vol 84. Pittsburgh, PA: Mater. Res. Soc; 1987. p. 493–507.
13. Gin S, Abdelouas A, Criscenti LJ, Ebert WL, Ferrand K, Geisler T, et al. An international initiative on long-term behavior of high-level nuclear waste glass. *Mater Today.* 2013;16(6):243–8.
14. Inagaki Y, Kikunaga T, Idemitsu K, Arima T. Initial dissolution rate of the international simple glass as a function of pH and temperature measured using microchannel flow-through test method. *Int J Appl Glass Sci.* 2013;4(4):317–27.
15. Geisler T, Janssen A, Scheiter D, Stephan T, Berndt J, Putnis A. Aqueous corrosion of borosilicate glass under acidic conditions: a new corrosion mechanism. *J Non Cryst Solids.* 2010;356(28–30):1458–65.
16. Wickert CL, Vieira AE, Dehne JA, Wang X, Wilder DM, Barkatt A. Effects of salts on silicate glass dissolution in water- kinetics and mechanisms of dissolution and surface cracking. *Phys Chem Glasses.* 1999;40(3):157–70.
17. Doremus RH. Interdiffusion of hydrogen and alkali ions in a glass surface. *J Non Cryst Solids.* 1975;19:137–44.
18. McGrail BP, Icenhower JP, Shuh DK, Liu P, Darab JG, Baer DR, et al. The structure of Na₂O-Al₂O₃-SiO₂ glass: impact on sodium ion exchange in H₂O and D₂O. *J Non Cryst Solids.* 2001;2001(296):10–26.

19. Ojovan MI, Pankov A, Lee WE. The ion exchange phase in corrosion of nuclear waste glasses. *J Nucl Mater.* 2006;358(1):57–68.
20. Gin S, Jollivet P, Fournier M, Angeli F, Frugier P, Charpentier T. Origin and consequences of silicate glass passivation by surface layers. *Nat Commun.* 2015;6.
21. Lenting C, Plümper O, Kilburn M, Guagliardo P, Klinkenberg M, Geisler T. Towards a unifying mechanistic model for silicate glass corrosion. *npj Mater Degrad.* 2018;2(1).
22. Gin S, Collin M, Jollivet J-P, Fournier M, Dupuy L, Mahadevan TS, et al. Dynamics of self-reorganization explains passivation of silicate glasses. *Nat Commun.* 2018;9:2169.
23. Geisler T, Dohmen L, Lenting C, Fritzsche MBK. Real-time in situ observations of reaction and transport phenomena during silicate glass corrosion by fluid-cell Raman spectroscopy. *Nat Mater.* 2019;18(4):342–8.
24. Geisler T, Nagel T, Kilburn MR, Janssen A, Icenhower JP, Fonseca ROC, et al. The mechanism of borosilicate glass corrosion revisited. *Geochim Cosmochim Acta.* 2015;158:112–29.
25. Angeli F, Gaillard M, Jollivet P, Charpentier T. Influence of glass composition and alteration solution on leached silicate glass structure : a solid-state NMR investigation. *Geochim Cosmochim Acta.* 2006;2006(70):2577–90.
26. Tite MS, Freestone I, Mason R, Molera J, Vendrell-Saz M, Wood N. Lead glazes in Antiquity - Methods of production and reasons for us. *Archaeometry.* 1998;40(2):241–60.
27. Freestone IC, Stapleton CP. Composition and technology of Islamic enamelled glass. In: Ward R, editor. *Gilded and enamelled glass from the Middle East.* British Museum Press; 1998.
28. Roisine G, Capobianco N, Caurant D, Wallez G, Bouquillon A, Majérous O, et al. The art of Bernard Palissy (1510–1590): influence of firing conditions on the microstructure of iron-coloured high-lead glazes. *Appl Phys A.* 2017;123(8).
29. Lehuédé P, Collin M, Dubus M. Techniques d'opacification de l'émail au XIX^e siècle : nouvel éclairage apporté par le microscope à balayage à effet de champ. *Technè.* 2015;42.
30. Lanmon DP, Whitehouse DB. Lampworked glass jewelry and figures In: Art TMMo, editor. *The Robert Lehman collection: The Metropolitan Museum of Art.* New York: Princeton University Press; 1993.
31. Alloteau F, Lehuédé P, Majérous O, Biron I, Dervanian A, Charpentier T, et al. New insight into atmospheric alteration of alkali-lime silicate glasses. *Corros Sci.* 2017;122:12–25.
32. Sessegolo L, Verney-Carron A, Saheb M, Remusat L, Gonzalez-Cano A, Nuns N, et al. Long-term weathering rate of stained-glass windows using H and O isotopes. *npj Mater Degrad.* 2018;2(1).
33. Lombardo T, Gentaz L, Verney-Carron A, Chabas A, Loisel C, Neff D, et al. Characterisation of complex alteration layers in medieval glasses. *Corros Sci.* 2013;72:10–9.
34. Abdelouas A, El Mendili Y, Ait Chaou A, Karakurt G, Hartnack C, Bardeau J-F, et al. A Preliminary Investigation of the ISG Glass Vapor Hydration. *Int J Appl Glass Sci.* 2013;4(4):307–16.
35. Abrajano TA Jr, Bates JK, Mazer JJ. Aqueous corrosion of natural and nuclear waste glasses. II. Mechanisms of vapor hydration of nuclear waste glasses. *J Non Cryst Solids.* 1989;1989(108):269–88.
36. Neeway J, Abdelouas A, Grambow B, Schumacher S, Martin C, Kogawa M, et al. Vapor hydration of SON68 glass from 90°C to 200°C: a kinetic study and corrosion products investigation. *J Non Cryst Solids.* 2012;358(21):2894–905.
37. Ojovan MI. On Alteration rate renewal stage of nuclear waste glass corrosion. *MRS Advances.* 2020;5(3–4):111–20.
38. Ojovan MI, Lee WE, Barinov AS, Ojovan NV, Startceva IV, Bacon DH, et al. Corrosion mechanisms of low level vitrified radioactive waste in a loamy soil. In: Hanchar JM, Stroes-Gascoyne, LB, editors. *Scientific basics for nuclear waste management XXVIII.* 824 ed, 2004. p. 333–8.
39. Sobolev IA, Ojovan MI, Batyukhnova OG, Ojovan NV, Scherbatova TD. Waste glass leaching and alteration under conditions of open site tests. In: Gray WJ, Triay IR, editors. *Scientific Basis for Nuclear Waste Management XX Symposium.* Pittsburgh, PA: Mater. Res. Soc; 1996. p. 245–52.
40. Narayanasamy S, Jollivet P, Godon N, Angeli F, Gin S, Cabié M, et al. Influence of composition of nuclear waste glasses on vapor phase hydration. *J Nucl Mater.* 2019;525:53–71.
41. Collin M, Fournier M, Frugier P, Charpentier T, Moskura M, Deng L, et al. Structure of international simple glass and properties of passivating layer formed in circumneutral pH conditions. *npj Mater Degrad.* 2018;2:4.
42. Pons-Corbeau J, Cazet JP, Moreau JP, Charbonnier JC. Quantitative surface analysis by glow discharge optical spectrometry. *Surf Interface Anal.* 1986;9(1):21–5.
43. Brossel M. Compréhension des mécanismes d'intégration du fer dans la couche d'altération du verre nucléaire - impact sur ses propriétés de transport et sa stabilité. Paris-Saclay University; 2017.
44. Massiot D, Fayon F, Capron M, King I, Le Calvé S, Alonso B, et al. Modelling one- and two-dimensional solid-state NMR spectra. *Magn Reson Chem.* 2002;40(1):70–6.
45. Hongo C, Tomita M, Takenaka M, Murakoshi A. Accurate SIMS depth profiling for ultra-shallow implants using backside SIMS. *Appl Surf Sci.* 2003;203–204:264–7.
46. Collin M, Fournier M, Charpentier T, Moskura M, Gin S. Impact of alkali on the passivation of silicate glass. *npj Mater Degrad.* 2018;2(16):16.
47. Collin M, Gin S, Jollivet P, Dupuy L, Dauvois V, Duffours L. ToF-SIMS depth profiling of altered glass. *npj Mater Degrad.* 2019;3(1).
48. Bronnimann CE, Zeigler RC, Maciel GE. Proton NMR study of dehydration of the silica gel surface. *J Am Chem Soc.* 1988;110(7):2023–6.
49. Takahashi M, Mizoguchi K, Masuda K. Potential of phyllosilicate dehydration and dehydroxylation reactions to trigger earthquakes. *J Geophys Res.* 2009;114(B2).
50. Zheng Q, Zhang Y, Montazerian M, Gulbitten O, Mauro JC, Zanutto ED, et al. Understanding glass through differential scanning calorimetry. *Chem Rev.* 2019;119(13):7848–939.
51. Le Losq C, Cody GD, Mysen BO. Alkali influence on the water speciation and the environment of protons in silicate glasses revealed by ¹H MAS NMR spectroscopy. *Am Mineral.* 2015;100(2–3):466–73.
52. Xue X, Kanzaki M. Proton distributions and hydrogen bonding in crystalline and glassy hydrous silicates and related inorganic materials: insights from high-resolution solid-state nuclear magnetic resonance spectroscopy. *J Am Ceram Soc.* 2009;92(12):2803–30.
53. Alloteau F, Majérous O, Biron I, Lehuédé P, Caurant D, Charpentier T, et al. Temperature-dependent mechanisms of the atmospheric alteration of a mixed-alkali lime silicate glass. *Corros Sci.* 2019;159:108129.
54. Protsak IS, Morozov YM, Dong W, Le Z, Zhang D, Henderson IM. A (29)Si, (1)H, and (13)C Solid-State NMR Study on the Surface Species of Various Depolymerized Organosiloxanes at Silica Surface. *Nanoscale Res Lett.* 2019;14(1):160.

55. Lareau RT, editor. Secondary Ion Mass Spectrometry SIMS VI1988; Chichester: Wiley.
56. Diallo B, Allix M, Véron E, Sarou-Kanian V, Bardez-Giboire I, Montouillout V, et al. Deconvolution method of ^{29}Si MAS NMR spectra applied to homogeneous and phase separated lanthanum aluminosilicate glasses. *J Non Cryst Solids*. 2019;503–504: 352–65.
57. Fournier M, Gin S, Frugier P. Resumption of nuclear glass alteration: State of the art. *J Nucl Mater*. 2014;448(1–3):348–63.
58. Ribet S, Gin S. Role of neoformed phases on the mechanisms controlling the resumption of SON68 glass alteration in alkaline media. *J Nucl Mater*. 2004;2004(324):152–64.
59. Caurel J, Beaufort D, Vernaz EY. Mineral phase identification along two profiles from the LWR French reference glass: use of an X-ray position sensitive detector. In: Apted MJ, Westerman RE, editors. *Scientific Basis for Nuclear Waste Management XI*. Pittsburgh, PA: Mater. Res. Soc; 1987. p. 663–72.
60. Koob S. Conservation and care of glass objects. New-York: Archetype edition; 2006.
61. Davison S, Newton RG. Conservation and restoration of glass: Butterworth edition. 2003.
62. Verhaar G. Glass sickness: Detection and prevention: Investigating unstable glass in museum collections, 2018.
63. Tsomaia N, Brantley SL, Hamilton JP, Pantano CG, Mueller KT. NMR evidence for formation of octahedral and tetrahedral Al and repolymerization of the Si network during dissolution of aluminosilicate glass and crystal. *Am Mineral*. 2003;88: 54–67.
64. Criscenti LJ, Brantley SL, Mueller KT, Tsomaia N, Kubicki JD. Theoretical and ^{27}Al CPMAS NMR investigation of aluminum coordination changes during aluminosilicate dissolution. *Geochim Cosmochim Acta*. 2005;69(9):2205–20.
65. Dirken PJ, Nachtgall GH, Kentgens APM. Off-resonance nutation nuclear magnetic resonance study of framework aluminosilicate glasses with Li, Na, K, Rb or Cs as charge-balancing cation. *Solid State Nucl Magn Reson*. 1995;5:189–200.
66. Du T, Li H, Zhou Q, Wang Z, Sant G, Ryan JV, et al. Atomistic origin of the passivation effect in hydrated silicate glasses. *npj Mater Degrad*. 2019;3(1).
67. Alloteau F. Contribution à la compréhension des mécanismes de l'altération atmosphérique des verres et étude d'un traitement de protection à base de sels de zinc. Université de recherche Paris Sciences et Lettres; 2017.
68. Mansas C, Delaye J-M, Charpentier T, Bruguier F, Bouty O, Penelon B, et al. Drivers of water transport in glass: chemical or topological effect of the glass network? *J Phys Chem C*. 2017;121(30):16201–15.
69. Liu H, Ngo D, Ren M, Du J, Kim SH. Effects of surface initial condition on aqueous corrosion of glass—a study with a model nuclear waste glass. *J Am Ceram Soc*. 2019;102(4):1652–64.
70. Sessegolo L, Verney-Carron A, Ausset P, Saheb M, Chabas A. Effect of surface roughness on medieval-type glass alteration in aqueous medium. *J Non Cryst Solids*. 2019;505:260–71.
71. Libourel G, Verney-Carron A, Morlok A, Gin S, Sterpenich J, Michelin A, et al. The use of natural and archeological analogues for understanding the long-term behavior of nuclear glasses. *Collect C R Geosci*. 2011;343(2–3):237–45.

SUPPORTING INFORMATION

Additional supporting information may be found online in the Supporting Information section.

How to cite this article: Collin M, Diallo B, Lecoq H, Ory S, Chauvet E, Pellerin N. Chemical durability of lead crystal glass: Comparison of short-term aqueous and atmospheric alteration at 90°C. *Int J Appl Glass Sci*. 2020;00:1–17. <https://doi.org/10.1111/ijag.15843>